Monthly Notices
of the
ROYAL ASTRONOMICAL SOCIETY

MNRAS **431,** 308–321 (2013) doi:10.1093/mnras/stt162
Advance Access publication 2013 February 23

Light curve and spectral evolution of the Type IIb supernova 2011fu

Brajesh Kumar,[1,2⋆] S. B. Pandey,[1] D. K. Sahu,[3] J. Vinko,[4] A. S. Moskvitin,[5] G. C. Anupama,[3] V. K. Bhatt,[1] A. Ordasi,[6] A. Nagy,[4] V. V. Sokolov,[5] T. N. Sokolova,[5] V. N. Komarova,[5] Brijesh Kumar,[1] Subhash Bose,[1] Rupak Roy[1] and Ram Sagar[1]

[1]*Aryabhatta Research Institute of Observational Sciences (ARIES), Manora Peak, Nainital 263129, India*
[2]*Institut d'Astrophysique et de Géophysique, Université de Liège, Allée du 6 Août 17, Bât B5c, B-4000 Liège, Belgium*
[3]*Indian Institute of Astrophysics, Koramangala, Bangalore 560 034, India*
[4]*Department of Optics and Quantum Electronics, University of Szeged, Dóm tér 9, Szeged, Hungary*
[5]*Special Astrophysical Observatory, Nizhnij Arkhyz, Karachaevo-Cherkesia, 369167 Russia*
[6]*Department of Experimental Physics, University of Szeged, Dóm tér 9, Szeged, Hungary*

Accepted 2013 January 25. Received 2013 January 24; in original form 2012 November 9

ABSTRACT

We present the low-resolution spectroscopic and *UBVRI* broad-band photometric investigations of the Type IIb supernova (SN) 2011fu, discovered in UGC 01626. The photometric follow-up of this event was initiated a few days after the explosion and covers a period of about 175 d. The early-phase light curve shows a rise, followed by steep decay in all bands, and shares properties very similar to that seen for SN 1993J, with a possible detection of the adiabatic cooling phase. Modelling of the quasi-bolometric light curve suggests that the progenitor had an extended ($\sim 1 \times 10^{13}$ cm), low-mass ($\sim 0.1\,M_{\odot}$) H-rich envelope on top of a dense, compact ($\sim 2 \times 10^{11}$ cm), more massive ($\sim 1.1\,M_{\odot}$) He-rich core. The nickel mass synthesized during the explosion was found to be $\sim 0.21\,M_{\odot}$, slightly larger than that seen for other Type IIb SNe. The spectral modelling performed with SYNOW suggests that the early-phase line velocities for H and Fe II features were $\sim 16\,000$ and $\sim 14\,000$ km s^{-1}, respectively. Then, the velocities declined up to day +40 and became nearly constant at later epochs.

Key words: supernovae: general – supernovae: individual: SN 2011fu – supernovae: individual (SN 1993J) – galaxies: individual (UGC 01626).

1 INTRODUCTION

It is commonly recognized that core-collapse supernovae (CCSNe) represent the final stages of the lives of massive stars ($M > 8$–$10\,M_{\odot}$; Heger et al. 2003; Anderson & James 2009; Smartt 2009). Generally, the fate of a massive star is governed by its mass, metallicity, rotation and magnetic field (Fryer 1999; Heger et al. 2003; Woosley & Janka 2005). Massive stars show a wide variety in these fundamental parameters, causing diverse observational properties among various types of CCSNe. The presence of dominant hydrogen lines in the spectra of Type II SNe strongly suggests that their progenitors belong to massive stars, which are still surrounded by significantly thick hydrogen envelopes before the explosion (for a review on different types of SNe, see Filippenko 1997). In contrast, Type Ib events are H-deficient, but He is still present in their spectra, unlike Type Ic SNe, where both H and He features are absent. After the discovery of SN 1987K, another class, termed Type IIb (see Woosley et al. 1987; Filippenko 1988), was included in the CCSN zoo. The observational properties of these SNe closely resemble those of Type II SNe during the early phases, while they are more similar to Type Ib/c events at later epochs.

However, in a few cases, the spectral classification of Type IIb SNe is more controversial: for example, SN 2000H (Benetti et al. 2000; Branch et al. 2002; Elmhamdi et al. 2006), SN 2003bg (Filippenko & Chornock 2003; Soderberg et al. 2006), SN 2007Y[1] and SN 2009mg (Prieto 2009; Roming, Prieto & Milne 2009a; Stritzinger 2010). Type IIb SNe are further divided into two subgroups: Type cIIb with compact progenitors, such as SNe 1996cb, 2001ig and 2008ax, and Type eIIb with extended progenitors, such as SNe 1993J and 2001gd (Chevalier & Soderberg 2010).

Type IIb and Type Ib/c SNe are collectively known as stripped envelope CCSNe (Clocchiatti et al. 1997) because the outer

⋆E-mail: brajesh@aries.res.in, brajesharies@gmail.com

[1] Although this event is classified as Type Ib/c by, for example, Monard (2007) and Stritzinger et al. (2009), Maurer et al. (2010) have suggested that it is Type IIb.

envelopes of hydrogen and/or helium of their progenitors are partially or completely removed before the explosion. The possible physical mechanisms behind this process might be stellar winds (Puls, Vink & Najarro 2008) or interaction with a companion star in a binary system, where mass transfer occurs as a result of Roche lobe overflow (Podsiadlowski, Joss & Hsu 1992). There have been several studies about the discovery of the progenitors of Type IIb SNe, but there is still a debate about how they manage to keep only a thin layer of hydrogen (Aldering, Humphreys & Richmond 1994; Maund et al. 2004; Ryder, Murrowood & Stathakis 2006; Crockett et al. 2008; Sonbas et al. 2008; Arcavi et al. 2011; Maund et al. 2011; Van Dyk et al. 2011; Soderberg et al. 2012).

To date, approximately 77[2] Type IIb SNe are known, but only a few of these have been properly monitored and well studied. Among these, SNe 1987K (Filippenko 1988), 1993J (Schmidt et al. 1993; Lewis et al. 1994; Richmond et al. 1994), 1996cb (Qiu et al. 1999), 2003bg (Hamuy et al. 2009; Mazzali et al. 2009), 2008ax (Pastorello et al. 2008; Roming et al. 2009b; Chornock et al. 2011; Taubenberger et al. 2011), 2009mg (Oates et al. 2012), 2011ei (Milisavljevic et al. 2012) and, more recently, 2011dh (Arcavi et al. 2011; Martí-Vidal et al. 2011; Maund et al. 2011; Van Dyk et al. 2011; Bersten et al. 2012; Bietenholz et al. 2012; Horesh et al. 2012; Krauss et al. 2012; Soderberg et al. 2012; Vinkó et al. 2012) have been remarkably well studied.

An interesting property of the observed light curves (LCs) of a few Type IIb SNe is the initial peak and rapid decline, followed by a subsequent rise and a secondary maximum. The first peak is thought to be a result of the break-out of the SN shock from the extended progenitor envelope (Falk & Arnett 1977). The properties of the shock break-out peak depend on the envelope mass and the density structure of the outer layers. The shock break-out phase can last from seconds to days. Therefore, early discovery and rapid-cadence early-time observations might help us to better understand the properties of the outer envelope of massive stars (Gal-Yam et al. 2011).

In this paper, we present the results from photometric and spectroscopic monitoring of SN 2011fu, starting shortly after the discovery and extending up to nebular phases. The photometric and spectroscopic properties of this event have revealed that SN 2011fu is a Type IIb SN. The type determination for this SN was verified with SNID (Blondin & Tonry 2007), highlighting the fact that the object has an excellent resemblance to SN 1993J.

The paper is organized as follows. We present the photometric and spectroscopic observations in Section 2, where we describe the methods for data reduction and analysis. In Section 3, we analyse the light and colour curves. In Section 4, we describe and model the bolometric LC. In Section 5, we deal with the spectroscopic modelling using the SYNOW code. In Section 6, we discuss the metallicities of the host galaxy of SN 2011fu, along with those of other CCSNe. Finally, we summarize our results in Section 7.

2 OBSERVATIONS AND DATA ANALYSIS

SN 2011fu was discovered in a spiral arm of the galaxy UGC 01626 – type SAB(rs)*c* – by F. Ciabattari and E. Mazzoni (Ciabattari et al. 2011) on 2011 September 21.04 (UT) with a 0.5-m Newtonian telescope, in the course of the Italian Supernovae Search Project. The brightness of the SN at the time of discovery was reported to be ∼16 mag (unfiltered). It was located 2 arcsec west and 26 arcsec north of the centre of the host galaxy, with coordinates $\alpha = 02^{\rm h}08^{\rm m}21\overset{\rm s}{.}41$, $\delta = +41^{\circ}29'12\overset{''}{.}3$ (equinox 2000.0; Ciabattari et al. 2011). The host galaxy has a heliocentric velocity and redshift of 5543 ± 11 km s^{-1} and $z = 0.018489 \pm 0.000037$,[3] respectively. The first spectrum of SN2011fu was obtained on 2011 September 23.84 UT with the Ekar-Copernico 1.82-m telescope (range 360–810 nm; resolution 2.2 nm) by Tomasella et al. (2011). This spectrum showed a blue continuum with superimposed weak H and He I 587.6-nm features, which led to the classification of a young Type II SN.

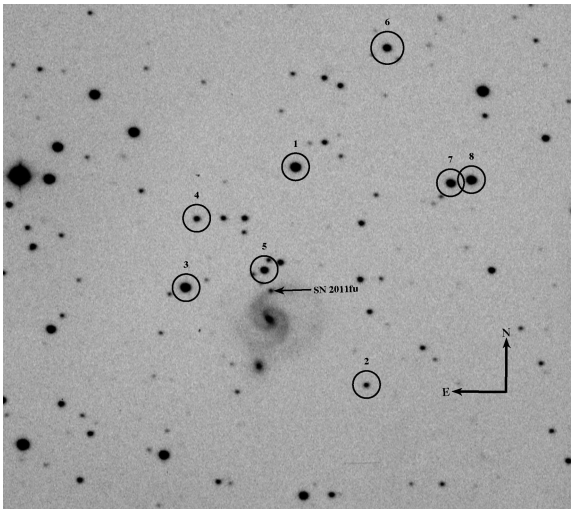

Figure 1. The *V*-band image of the SN 2011fu field around the galaxy UGC 01626, observed on 2011 November 16 with the 1-m ST, India. The SN is marked with a black arrow. The reference standard stars used for calibration are marked with numbers 1–8. On this image, north is up and east is to the left.

2.1 Optical photometry

The prompt photometric follow-up of SN 2011fu started shortly after the discovery and continued using three ground-based telescopes in India. The majority of the observations were made using the 2-m Himalayan Chandra Telescope (HCT) of the Indian Astronomical Observatory (IAO), Hanle, and the 1-m Sampurnanand Telescope (ST) at the Aryabhatta Research Institute of Observational Sciences (ARIES), Nainital, India. All observations were performed in Bessell *UBVRI* bands.

The HCT photometric observations started on 2011 September 28, using the Himalaya Faint Object Spectrograph Camera (HFOSC). The central 2k × 2k region of a 2k × 4k SITe CCD chip was used for imaging, which provided an image scale of 0.296 arcsec pixel^{-1} across a 10 × 10 arcmin^2 field of view.

Further photometric observations were carried out using a 2k × 2k CCD camera at the *f*/13 Cassegrain focus of the 1-m ST telescope, situated at ARIES, Nainital. The CCD chip has square pixels of 24 × 24 μm and a scale of 0.38 arcsec per pixel, and the entire chip covers a field of 13 × 13 arcmin^2 on the sky. The gain and readout noise of the CCD camera are 10 electrons per ADU and 5.3 electrons, respectively. Fig. 1 presents a finding chart, showing the field of the SN 2011fu along with the local standard stars.

[2] See http:heasarc.gsfc.nasa.gov/W3Browse/star-catalog/asiagosn.html.

[3] See HyperLEDA, http://leda.univ-lyon1.fr.

Table 1. Identification number (ID), coordinates (α, δ) and calibrated magnitudes of standard stars in the field of SN 2011fu.

Star ID	α_{J2000} (h m s)	δ_{J2000} ($^\circ$ $'$ $''$)	U (mag)	B (mag)	V (mag)	R (mag)	I (mag)
1	02 08 19.66	+41 30 53.4	15.59 ± 0.02	15.47 ± 0.02	14.80 ± 0.01	14.38 ± 0.02	14.03 ± 0.02
2	02 08 14.25	+41 27 51.8	18.39 ± 0.09	18.17 ± 0.02	17.59 ± 0.02	17.16 ± 0.02	16.83 ± 0.03
3	02 08 27.70	+41 29 11.4	16.29 ± 0.02	15.70 ± 0.02	14.86 ± 0.02	14.34 ± 0.02	13.93 ± 0.03
4	02 08 26.92	+41 30 07.5	17.53 ± 0.04	17.58 ± 0.02	17.07 ± 0.02	16.70 ± 0.02	16.40 ± 0.03
5	02 08 21.94	+41 29 26.9	16.78 ± 0.03	16.77 ± 0.02	16.21 ± 0.01	15.84 ± 0.02	15.54 ± 0.02
6	02 08 12.72	+41 32 34.8	16.36 ± 0.02	16.45 ± 0.02	15.85 ± 0.01	15.44 ± 0.02	15.07 ± 0.02
7	02 08 08.04	+41 30 41.3	16.32 ± 0.02	16.07 ± 0.02	15.38 ± 0.01	14.97 ± 0.02	14.61 ± 0.02
8	02 08 06.54	+41 30 43.7	17.23 ± 0.03	16.03 ± 0.02	14.93 ± 0.02	14.32 ± 0.02	13.78 ± 0.02

In addition, we also observed this SN in the V and R bands on 2011 December 01 and 2012 March 02 using the 1.3-m Devasthal Fast Optical Telescope[4] (DFOT; Sagar et al. 2011, 2012), recently installed at Devasthal, Naintial.

To improve the signal-to-noise ratio (S/N), all the photometric observations were carried out with 2×2 binning. Along with science frames, several bias and twilight flat frames were also collected. Alignment and determination of mean FWHM on all science frames were performed after the usual bias-subtraction, flat-fielding and cosmic ray removal. The standard tasks available in IRAF[5] and DAOPHOT[6] (Stetson 1987, 1992) were used for pre-processing and photometry.

The pre-processing steps for images taken with all three telescopes were performed in a similar fashion. The stellar FWHM on the V-band frames typically varied from 2 to 4 arcsec, with a median value of around 2.5 arcsec. We also co-added individual frames, wherever necessary, before computing the final photometry.

For photometric calibration, we observed the standard field PG0231 (Landolt 2009) in *UBVRI* bands with the 1-m ST on 2011 December 17 under good photometric conditions (transparent sky, seeing FWHM in $V \sim 2$ arcsec). The profile fitting technique was applied for the photometry of SN 2011fu and Landolt field, and then instrumental magnitudes were converted into the standard system, following the least-squares linear regression procedures outlined by Stetson (1992). Atmospheric extinction values (0.57, 0.28, 0.17, 0.11 and 0.07 mag per unit airmass for the U, B, V, R and I bands, respectively) for the site were adopted from Kumar et al. (2000). The chosen Landolt stars for calibration had a brightness range of $12.77 \leq V \leq 16.11$ mag and colour range of $-0.33 \leq B - V \leq 1.45$ mag. Using these stars, transformation to the standard system was derived by applying the following zero-points and colour coefficients:

$$u - U = (7.27 \pm 0.01) + (-0.08 \pm 0.02)(U - B);$$

$$b - B = (4.90 \pm 0.004) + (-0.04 \pm 0.01)(B - V);$$

$$v - V = (4.34 \pm 0.01) + (-0.04 \pm 0.01)(B - V);$$

$$r - R = (4.19 \pm 0.01) + (-0.04 \pm 0.01)(V - R);$$

$$i - I = (4.60 \pm 0.02) + (0.04 \pm 0.02)(V - I).$$

Here, U, B, V, R and I are the catalogue magnitudes and u, b, v, r and i are the corresponding instrumental magnitudes. Table 1 lists the coordinates and magnitudes of the eight local secondary standard stars in the SN field.

To estimate the possible contribution from the host galaxy to the measured SN fluxes, we used the ISIS[7] image subtraction package. We acquired deep images (having total exposure times of more than 20 min) in the *BVRI* bands with the HCT on 25 August 2012 under good sky conditions. Because the SN was not detected in any of these frames, we used them as template frames for image subtraction. We found minor differences, not exceeding 0.1 mag, between the SN magnitudes with and without applying the image subtraction for the data at later epochs (i.e. 70 d after the first observation). Table 2 presents the final results of our SN photometry (without applying image subtraction corrections) along with robustly determined point spread function errors.

2.2 Spectroscopy

Spectroscopic observations of SN 2011fu were obtained at eight epochs, between 2011 September 28 (JD 2455833.27) and December 22 (JD 2455918.11). A journal of these observations is given in Table 3. The SN spectra were taken with the HFOSC mounted at the 2-m HCT. All spectra were obtained using grisms Gr#7 (wavelength range 3500–7800 Å) and Gr#8 (wavelength range 5200–9200 Å). FeAr and FeNe arc lamp spectra were applied for wavelength calibration. Spectrophotometric standards were also observed with a broader slit to correct for the instrumental response and flux calibration.

The reduction of the spectroscopic data was carried out in a standard manner, using various tasks available within IRAF. First, all images were bias-subtracted and flat-fielded. Then, one-dimensional

[4] The DFOT uses a 2048 × 2048 ANDOR CCD camera, having 13.5 × 13.5 μm pixels mounted at the *f*/4 Cassegrain focus of the telescope. With a 0.54 arcsec pixel^{-1} plate scale, the entire chip covers a 18 × 18 arcmin^2 field of view on the sky. The CCD can be read out with 31, 62, 500 and 1000 kHz speeds, with system rms noise of 2.5, 4.1, 6.5 and 7 electrons and gain of 0.7, 1.4, 2 and 2 electron ADU^{-1}, respectively. We selected the 500-kHz readout frequency during our observations.

[5] IRAF is the Image Reduction and Analysis Facility distributed by the National Optical Astronomy Observatories, which is operated by the Association of Universities for research in Astronomy, Inc., under cooperative agreement with the National Science Foundation.

[6] DAOPHOT stands for Dominion Astrophysical Observatory Photometry.

[7] http://www2.iap.fr/users/alard/package.html

Table 2. Photometric observational log of SN 2011fu.

JD	Phase[a] (d)	*U* (mag)	*B* (mag)	*V* (mag)	*R* (mag)	*I* (mag)	Telescope[b]
2455833.23	+10.73	17.36 ± 0.03	17.68 ± 0.02	17.35 ± 0.01	16.99 ± 0.02	16.74 ± 0.02	HCT
2455834.49	+11.99	17.66 ± 0.03	17.87 ± 0.02	17.48 ± 0.01	17.11 ± 0.02	16.86 ± 0.02	HCT
2455836.15	+13.65	–	17.92 ± 0.03	17.46 ± 0.01	17.08 ± 0.02	16.88 ± 0.02	HCT
2455837.26	+14.76	17.73 ± 0.03	17.89 ± 0.02	17.42 ± 0.01	17.02 ± 0.02	16.83 ± 0.02	HCT
2455841.23	+18.73	17.65 ± 0.03	17.65 ± 0.02	17.15 ± 0.01	16.77 ± 0.02	16.59 ± 0.02	ST
2455842.30	+19.80	17.69 ± 0.05	17.63 ± 0.03	17.07 ± 0.01	16.70 ± 0.02	16.56 ± 0.03	ST
2455843.27	+20.77	17.62 ± 0.09	17.51 ± 0.05	17.05 ± 0.02	16.67 ± 0.02	16.57 ± 0.04	ST
2455844.21	+21.71	17.48 ± 0.06	17.49 ± 0.03	17.01 ± 0.02	16.62 ± 0.02	16.48 ± 0.03	ST
2455845.44	+22.94	17.43 ± 0.03	17.48 ± 0.03	16.95 ± 0.02	16.59 ± 0.02	16.45 ± 0.03	ST
2455845.43	+22.93	–	17.43 ± 0.02	16.93 ± 0.01	16.54 ± 0.02	16.43 ± 0.02	HCT
2455846.44	+23.94	17.51 ± 0.03	17.47 ± 0.03	16.92 ± 0.02	16.57 ± 0.02	16.43 ± 0.03	ST
2455846.43	+23.93	–	17.45 ± 0.02	16.92 ± 0.01	16.54 ± 0.02	16.45 ± 0.02	HCT
2455849.41	+26.91	17.68 ± 0.03	17.58 ± 0.03	16.95 ± 0.01	16.53 ± 0.02	16.38 ± 0.02	HCT
2455850.40	+27.89	17.76 ± 0.04	17.65 ± 0.03	16.96 ± 0.01	16.57 ± 0.02	16.43 ± 0.03	HCT
2455851.31	+28.81	18.21 ± 0.13	17.82 ± 0.04	17.06 ± 0.03	16.56 ± 0.02	16.44 ± 0.03	ST
2455857.30	+34.80	18.99 ± 0.06	18.52 ± 0.03	17.44 ± 0.01	16.80 ± 0.02	16.58 ± 0.03	ST
2455858.32	+35.82	19.00 ± 0.09	18.60 ± 0.03	17.47 ± 0.01	16.84 ± 0.02	16.61 ± 0.03	ST
2455859.18	+36.68	–	18.74 ± 0.03	17.51 ± 0.01	16.92 ± 0.02	16.69 ± 0.02	HCT
2455860.30	+37.80	19.10 ± 0.08	18.73 ± 0.03	17.60 ± 0.01	16.93 ± 0.02	16.68 ± 0.02	ST
2455862.30	+39.80	19.24 ± 0.15	18.86 ± 0.03	17.69 ± 0.02	16.97 ± 0.02	16.71 ± 0.03	ST
2455864.40	+41.90	19.55 ± 0.08	19.05 ± 0.03	17.77 ± 0.01	17.09 ± 0.02	16.84 ± 0.02	HCT
2455865.35	+42.85	–	19.12 ± 0.02	17.81 ± 0.01	17.11 ± 0.02	16.85 ± 0.02	HCT
2455866.23	+43.73	–	18.97 ± 0.05	17.88 ± 0.02	17.14 ± 0.02	16.83 ± 0.03	ST
2455866.26	+43.76	–	19.10 ± 0.02	17.86 ± 0.02	17.17 ± 0.02	16.88 ± 0.02	HCT
2455875.22	+52.72	–	–	18.06 ± 0.06	17.33 ± 0.04	16.95 ± 0.05	ST
2455879.28	+56.78	–	19.30 ± 0.10	18.17 ± 0.03	17.55 ± 0.03	17.18 ± 0.03	ST
2455881.26	+58.76	–	–	18.19 ± 0.02	17.50 ± 0.02	17.18 ± 0.03	HCT
2455882.33	+59.83	–	19.38 ± 0.07	18.19 ± 0.03	17.56 ± 0.02	17.20 ± 0.03	ST
2455884.27	+61.78	19.94 ± 0.05	19.49 ± 0.03	18.28 ± 0.01	17.62 ± 0.01	17.30 ± 0.02	HCT
2455894.23	+71.73	19.67 ± 0.20	19.37 ± 0.05	18.41 ± 0.03	17.76 ± 0.02	17.42 ± 0.03	ST
2455896.28	+73.78	19.75 ± 0.07	19.49 ± 0.03	18.43 ± 0.01	17.87 ± 0.02	17.57 ± 0.03	HCT
2455897.08	+74.58	–	–	18.39 ± 0.03	17.79 ± 0.03	–	DFOT
2455898.30	+75.80	–	19.28 ± 0.05	18.41 ± 0.02	17.79 ± 0.02	17.45 ± 0.03	ST
2455900.17	+77.66	–	19.47 ± 0.08	18.50 ± 0.03	17.83 ± 0.03	17.53 ± 0.03	ST
2455901.24	+78.74	–	19.36 ± 0.06	18.48 ± 0.04	17.88 ± 0.03	17.39 ± 0.03	ST
2455904.28	+81.78	–	19.31 ± 0.17	–	17.97 ± 0.05	17.72 ± 0.04	HCT
2455909.18	+86.68	–	19.52 ± 0.07	18.60 ± 0.03	17.96 ± 0.03	17.63 ± 0.03	ST
2455912.28	+89.78	–	19.45 ± 0.05	18.64 ± 0.03	18.06 ± 0.03	17.67 ± 0.04	ST
2455913.24	+90.73	19.56 ± 0.12	19.47 ± 0.05	18.59 ± 0.03	18.09 ± 0.03	17.70 ± 0.03	ST
2455918.18	+95.68	–	19.55 ± 0.03	–	18.21 ± 0.03	17.82 ± 0.03	HCT
2455919.11	+96.61	–	19.58 ± 0.04	18.75 ± 0.01	18.22 ± 0.02	17.87 ± 0.02	HCT
2455922.17	+99.67	–	19.48 ± 0.06	18.74 ± 0.03	18.24 ± 0.03	17.81 ± 0.04	ST
2455924.10	+101.60	–	19.65 ± 0.03	18.86 ± 0.01	18.34 ± 0.02	18.02 ± 0.02	HCT
2455929.17	+106.67	–	19.73 ± 0.09	18.92 ± 0.04	18.36 ± 0.05	18.00 ± 0.04	ST
2455930.27	+107.76	–	–	19.04 ± 0.11	18.47 ± 0.07	17.99 ± 0.12	ST
2455930.27	+108.73	–	–	18.89 ± 0.15	18.29 ± 0.10	17.93 ± 0.10	ST
2455932.15	+109.65	–	19.80 0.16	19.00 ± 0.05	–	18.11 ± 0.03	HCT
2455936.25	+113.75	–	–	–	–	18.27 ± 0.06	HCT
2455937.16	+114.66	–	19.69 ± 0.09	19.09 ± 0.04	18.58 ± 0.03	18.13 ± 0.04	HCT
2455938.08	+115.58	–	19.70 ± 0.04	19.11 ± 0.02	18.65 ± 0.03	18.35 ± 0.03	HCT
2455939.23	+116.73	–	–	19.00 ± 0.07	–	18.11 ± 0.05	ST
2455947.06	+124.56	–	–	19.21 ± 0.02	18.74 ± 0.02	18.46 ± 0.04	HCT
2455947.16	+124.66	–	–	–	18.55 ± 0.04	18.16 ± 0.07	ST
2455953.08	+130.58	–	19.64 ± 0.08	–	18.68 ± 0.03	18.38 ± 0.06	ST
2455954.16	+131.66	–	–	19.33 ± 0.02	18.87 ± 0.02	18.49 ± 0.03	HCT
2455963.14	+140.64	–	–	19.23 ± 0.07	–	18.54 ± 0.10	ST
2455967.11	+144.61	–	–	19.18 ± 0.07	18.87 ± 0.05	18.48 ± 0.08	ST
2455969.09	+146.59	–	–	–	18.91 ± 0.05	–	ST
2455976.07	+153.56	–	–	19.40 ± 0.03	18.88 ± 0.03	18.58 ± 0.07	ST
2455979.12	+156.62	–	–	–	18.92 ± 0.05	18.51 ± 0.09	ST
2455989.08	+166.58	–	–	19.59 ± 0.09	19.24 ± 0.10	18.87 ± 0.08	DFOT, ST
2455998.08	+175.58	–	–	–	19.07 ± 0.05	18.89 ± 0.10	ST
2456159.34	+336.84	–	>22.5	>22	>21.5	>21	HCT

[a]With reference to the explosion epoch JD 2455822.5

[b]The abbreviations denote the following: HCT, 2-m Himalayan Chandra Telescope, IAO, Hanle; DFOT, 1.3-m Devasthal Fast Optical Telescope, ARIES, India; ST, 1-m Sampurnanand Telescope, ARIES, India.

Table 3. Log of spectroscopic observations of SN 2011fu.

Date	JD	Phase[a] (d)	Range (Å)	Resolution (Å)
2011-09-28	2455833.28	+10.78	3500–7800; 5200–9250	7
2011-09-29	2455834.41	+11.92	3500–7800; 5200–9250	7
2011-10-01	2455836.23	+13.73	3500–7800; 5200–9250	7
2011-10-14	2455849.43	+26.93	3500–7800; 5200–9250	7
2011-10-29	2455864.41	+41.91	3500–7800; 5200–9250	7
2011-10-31	2455866.36	+43.86	3500–7800; 5200–9250	7
2011-11-23	2455889.15	+66.65	3500–7800; 5200–9250	7
2011-12-22	2455918.11	+95.61	3500–7800	7

[a]With reference to the explosion epoch JD 2455822.5.

spectra were extracted from the two-dimensional cleaned images using the optimal extraction algorithm (Horne 1986). The wavelength calibration was computed using the arc spectra mentioned above. The accuracy of the wavelength calibration was checked using the night-sky emission lines, and small shifts were applied to the observed spectra whenever required. The instrumental response curves were determined using the spectrophotometric standards observed on the same night as the SN, and the SN spectra were calibrated to a relative flux scale. When the spectrophotometric standards could not be observed, the response curve based on observations on a night close in time to the SN observation was adopted. The flux-calibrated spectra in the two regions were combined to a weighted mean to obtain the final spectrum on a relative flux scale.

Finally, the spectra were brought to an absolute flux scale using zero-points determined from the calibrated, broad-band *UBVRI* magnitudes. The SN spectra were also corrected for the redshift of the host galaxy ($z = 0.018$), and dereddened assuming a total reddening of $E(B - V) = 0.22$ mag (see Section 3.3). The telluric lines have not been removed from the spectra.

3 LIGHT CURVES OF SN 2011FU

In this section, we present the multiband LCs of SN 2011fu, comparing them with the LCs of SN 1993J, and focusing on their temporal properties. We briefly discuss the explosion epoch of SN 2011fu in Section 3.1.

3.1 Explosion epoch of SN 2011fu

The detection of very early time LC features of SN 2011fu, similar to those seen for SN 1993J, indicates a very young age at the time of discovery. The very sharp rise followed by a relatively fast decline can be explained as the detection of the cooling phase, and this depends mainly on the ^{56}Ni mixing and the progenitor radius, as shown by hydrodynamical models of H-stripped CCSNe (Shigeyama et al. 1994; Woosley et al. 1994; Blinnikov et al. 1998; Bersten et al. 2012). For example, in the case of SN 2011dh, for a progenitor radius of <300 R$_\odot$, the cooling phase ends $\sim$5 d after the explosion (see fig. 10 of Bersten et al. 2012).

In the literature, the first detection of SN 2011fu was reported to be 2011 September 20.708 (Z. Jin and X. Gao, Mt Nanshan, China). However, according to Ciabattari et al. (2011), this object was not visible on 2011 August 10 at the SN location, putting a stringent limit on the explosion date. We have collected the following pieces of evidence to put a constraint on the explosion date of SN 2011fu.

(i) For CCSNe of Types Ib and IIb, the explosion dates have been estimated to be $\sim$20 d prior to the *V*-band maxima (Richardson, Branch & Baron 2006; Drout et al. 2011; see also Milisavljevic et al. 2012).

(ii) Type IIb SNe also exhibit bluer $B - V$ colour $\sim$40 d after the explosion (Pastorello et al. 2008), giving an indication about the explosion epoch.

(iii) The SNID (Blondin & Tonry 2007) fitting on the initial four spectra of SN 2011fu indicates that the explosion of this event would have occurred around 2011 September 20. However, the SNID fit for the later three epochs of the spectra (after the *V*-band maximum) points to 2011 September 17 as the explosion date.

(iv) In some well-studied Type IIb SNe, the explosion epoch is better constrained (e.g. SN 1993J, SN 2008ax and SN 2011dh) and their early LC features indicate that the adiabatic cooling phase might be observable for several days after the explosion and that this duration depends upon the volume of the photospheric shell (Roming et al. 2009b), as determined for SN 1993J (Wheeler et al. 1993; Lewis et al. 1994; Barbon et al. 1995), SN 2008ax (Roming et al. 2009b) and SN 2011dh (Arcavi et al. 2011).

Based on the above evidence, we have adopted 2011 September 18 ± 2 as the explosion epoch for SN 2011fu, and we use this for the following discussion in this paper.

3.2 Light-curve analysis

In Fig. 2, we plot the calibrated *UBVRI* LCs of SN 2011fu. The LCs span $\sim$175 d after the explosion. It is clear from Fig. 2 that the photometric observations of this SN started shortly after the explosion, showing the early declining phase in all bands. This is possibly related to the cooling tail after the shock break-out from an extended progenitor envelope (Chevalier 1992; Waxman, Mészáros & Campana 2007; Chevalier & Fransson 2008; Nakar & Sari 2010). The LCs of SN 2011fu are strikingly similar to those of SN 1993J, in both the initial and the following phases, exhibiting valley-like structures followed by rising peaks in all bands. At late epochs, the LCs are monotonically decreasing in all bands, as expected for expanding, cooling ejecta heated by only the radioactive decay of ^{56}Ni and ^{56}Co.

Beside SNe 1993J and 2011dh, SN 2011fu is the third known case among Type IIb SNe to date, where all the initial decline phases, the rise of the broader secondary peaks and the final declines have been observed – although Roming et al. (2010) have reported similar observations for SN 2008ax. In the following, we refer to the first minimum of the LC (when the initial decline stops and the rise to the secondary maximum starts) as the 'valley'.

To determine the epochs of the valleys (t_v, in d), the subsequent peaks (t_p, in d) and their corresponding brightness values, using a χ^2 minimization technique, we fitted a third-order polynomial to the LCs of both SN 2011fu and SN 1993J. The errors in the fitting procedure were estimated by the error propagation method. We have taken 1993 March 27.5 as the explosion date for SN 1993J (Wheeler et al. 1993). The derived values of t_v and t_p and the corresponding brightness values for both SNe are listed in Table 4.

The values of t_v and t_p for both SNe are similar within the errors in all the bands. However, for both SNe, the LCs peak earlier in the blue bands than in the red bands (see Table 4), which is a common feature seen in CCSNe. By applying the linear regression method, the decline and rising rates (in mag d^{-1}) were also estimated for three phases: the pre-valley (α_1), the valley-to-peak (α_2) and the after-peak (α_3) phases. The results of the fitting are shown in Table 5.

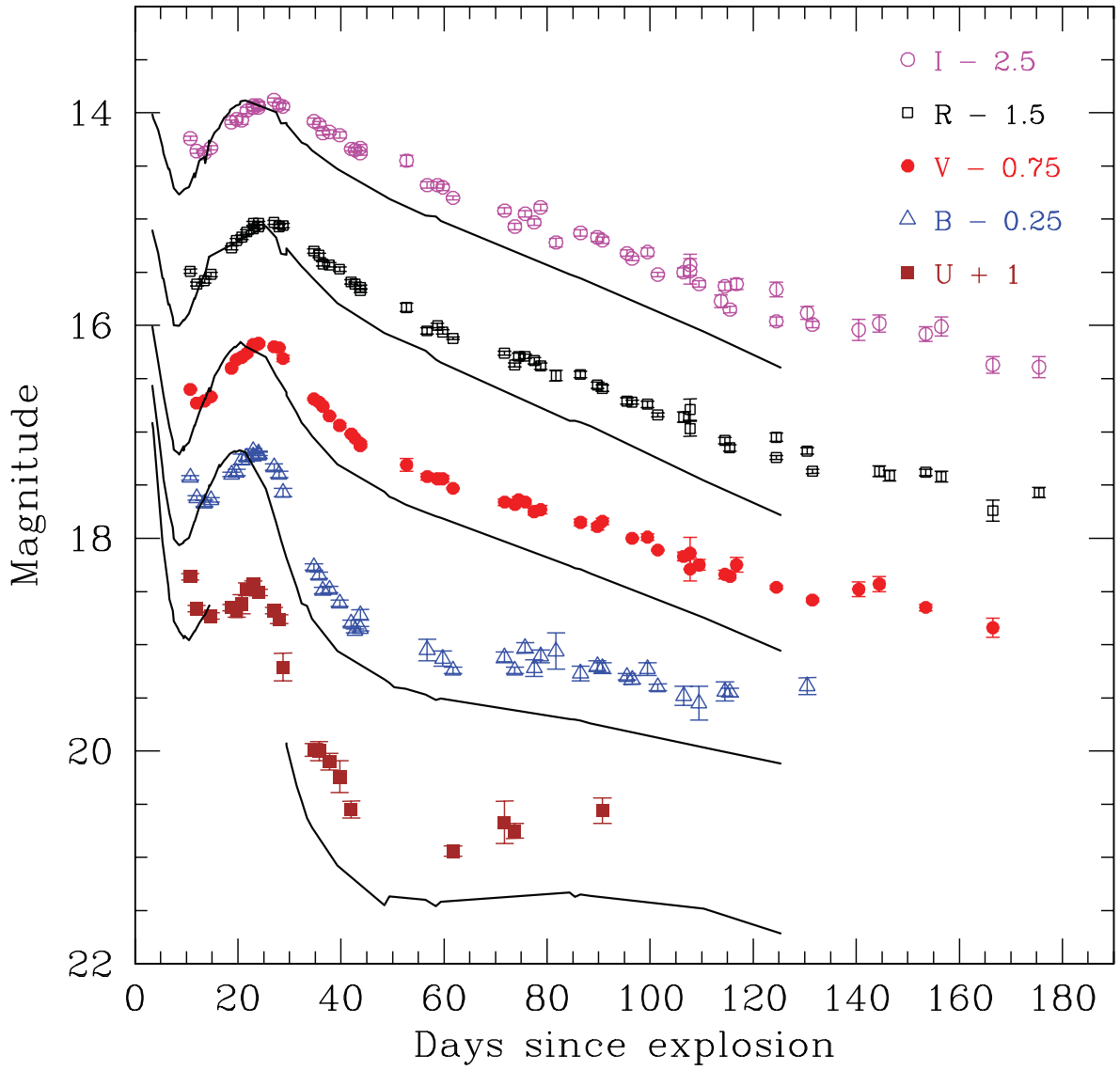

Figure 2. Observed *UBVRI* LCs of SN 2011fu. For clarity, the LCs in different bands have been shifted vertically by the values indicated in the legend. Black solid lines represent the LCs of SN 1993J overplotted with appropriate shifts. The explosion date of SN 2011fu was taken to be 2011 September 18 ± 2, as described in Section 3.1.

Table 4. Epochs of the LC valley (t_v) and the secondary peak (t_p) in days after the explosion, and their respective apparent magnitudes for SN 2011fu and SN 1993J.

SN	Band	LC valley t_v (d)	Apparent magnitude at t_v	LC peak t_p (d)	Apparent magnitude at t_p
	U	15.51 ± 4.34	17.67 ± 0.42	22.93 ± 3.64	17.43 ± 3.34
	B	13.75 ± 1.47	17.93 ± 0.80	23.29 ± 2.89	17.51 ± 0.83
2011fu	*V*	12.87 ± 1.69	17.45 ± 1.32	24.96 ± 2.01	16.95 ± 0.42
	R	12.95 ± 1.81	17.01 ± 1.20	26.40 ± 2.90	16.50 ± 0.11
	I	13.50 ± 1.89	16.86 ± 0.67	26.64 ± 2.80	16.41 ± 0.32
	U	10.33 ± 1.52	11.94 ± 0.76	–	–
	B	8.82 ± 3.36	12.27 ± 1.74	19.92 ± 0.70	11.40 ± 0.17
1993J	*V*	8.96 ± 1.41	11.89 ± 1.14	21.67 ± 0.66	10.87 ± 0.12
	R	8.81 ± 1.06	11.47 ± 0.61	22.53 ± 3.24	10.52 ± 0.37
	I	9.17 ± 1.58	11.25 ± 0.93	23.06 ± 1.91	10.39 ± 0.21

Table 5. Magnitude decay rate (in mag d^{-1}) before the valley (α_1), the rising rate between valley-to-peak (α_2) and the decay rate after the peak (α_3) for SN 2011fu and SN 1993J.

SN	Band	Decay rate before valley (α_1)	Rising rate between valley-to-peak (α_2)	Decay rate after peak (α_3)
	U	0.24 ± 0.05	-0.04 ± 0.01	0.13 ± 0.01
	B	0.15 ± 0.02	-0.05 ± 0.01	0.10 ± 0.01
2011fu	*V*	0.11 ± 0.03	-0.06 ± 0.01	0.05 ± 0.01
	R	0.09 ± 0.02	-0.05 ± 0.01	0.04 ± 0.01
	I	0.09 ± 0.02	-0.03 ± 0.01	0.02 ± 0.01
	U	0.38 ± 0.03	–	–
	B	0.24 ± 0.02	-0.08 ± 0.01	0.11 ± 0.01
1993J	*V*	0.24 ± 0.01	-0.10 ± 0.01	0.06 ± 0.01
	R	0.20 ± 0.01	–	–
	I	0.16 ± 0.01	-0.09 ± 0.01	0.05 ± 0.01

These values suggest that, for SN 2011fu, the pre-valley decay rates (α_1) are steeper (i.e. the decay is faster) at shorter wavelengths. This is also true for SN 1993J, where the decay rates (α_1) are even steeper. Thus, the initial LC decay of SN 1993J was steeper than that of SN 2011fu during this early phase (see also Barbon et al. 1995). Between the valley-to-peak phase (α_2), the LC of SN 2011fu evolved with a similar rate in all bands, but slower than that seen for SN 1993J. During the post-peak phase, the LCs gradually became flatter at longer wavelengths (see the α_3 values in Table 5). This trend has also been observed for SN 1993J and other Type IIb SNe. The *B*-band LC of SN 2011fu between 50 and 100 d after the explosion might even show a plateau, similar to SNe 1993J (see fig. 3 of Lewis et al. 1994) and 1996cb (see fig. 2 and the discussions of Qiu et al. 1999). The plateau-like behaviour of the *U*-band LC of the SN 2011fu event is more prominent than the *U*-band LC of SN 1993J.

We have also determined the Δm_{15} parameter for the *V*-band LCs of both SNe; Δm_{15} is defined as the decline in magnitude after 15 d post-maximum. We have found $\Delta m_{15}(V) = 0.75$ mag for SN 2011fu, which is slightly lower than that for SN 1993J [$\Delta m_{15}(V) = 0.9$ mag]. Both values are consistent with the mean $\Delta m_{15}(V) \sim 0.8 \pm 0.1$ mag for Type Ib/c SNe (Drout et al. 2011).

3.3 Colour evolution and reddening towards SN 2011fu

In Fig. 3, we compare the evolution of the optical colour indices of SN 2011fu with those of other Type IIb SNe. While constructing the colour curves, we interpolated the measured data points (listed in Table 2) wherever necessary. Before plotting the colours, reddening corrections were applied to all the bands. We have adopted $E(B-V) = 0.068$ mag as the reddening resulting from Milky Way interstellar matter in the direction of SN 2011fu (Schlegel, Finkbeiner & Davis 1998). The empirical correlation given by Munari & Zwitter (1997) was used to estimate the SN host galaxy extinction based on the measured Na I D lines. For this purpose, we calculated the weighted equivalent width (EW) of the unresolved Na I D absorption feature in the three spectra (taken on 2011 October 01, 14 and 31; see the log in Table 3), resulting in EW (Na I D) $\sim 0.35 \pm 0.29$ Å. This corresponds to $E(B-V) \sim 0.15 \pm 0.11$ mag, according to the relation given by Munari & Zwitter (1997). Finally, we adopted the sum of the two components, total $E(B-V) = 0.22 \pm 0.11$ mag, as the reddening in the direction of SN 2011fu.

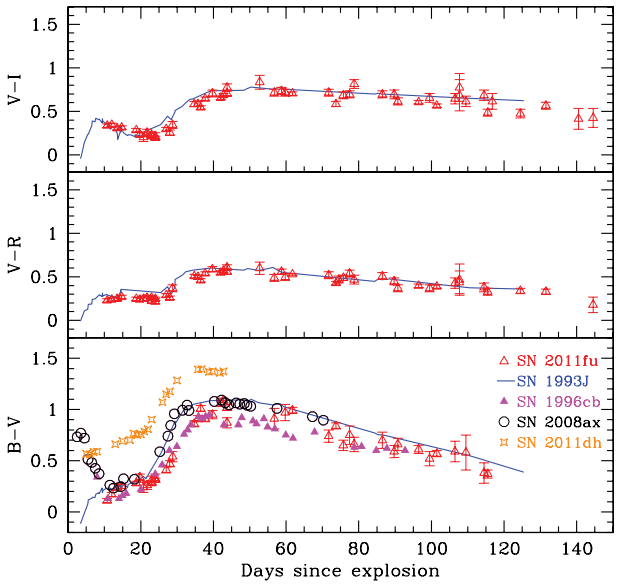

Figure 3. Colour curves of SN 2011fu and other Type IIb SNe. Bottom panel: $B-V$ colour evolution for SNe 2011fu, 2011dh, 2008ax, 1996cb (symbols) and 1993J (solid line). Middle panel: $V-R$ colour for SN 2011fu and SN 1993J. Top panel: the same the other panels but for $V-I$ colour.

The bottom panel of Fig. 3 shows the $B-V$ colour evolution of SN 2011fu, along with that of SNe 1993J (Lewis et al. 1994), 1996cb (Qiu et al. 1999), 2008ax (Pastorello et al. 2008) and 2011dh (Vinkó et al. 2012). We can see in Fig. 3 that the colour curves of SN 2011fu are similar to those of the majority of well-observed Type IIb SNe, except for SN 2011dh, which looks redder than the others.

Similar to SN 1993J, the initial $B-V$ colour of SN 2011fu increased (reddened) during the first 10 d (note that, during the same phase, SNe 2008ax and 1996cb showed the opposite trend). Between days +10 and +40, the $B-V$ colour continued to redden, and then after day +40 it started to decrease and became bluer until the end of the our observations. This type of colour evolution seems to be a common trend for Type Ib/c and IIb SNe. It might suggest that the SN ejecta became optically thin after 40 d. The $V-R$ (middle panel) and $V-I$ (upper panel) colour indices evolve with a similar trend as the $B-V$ colour.

3.4 Comparison of absolute magnitudes

The distribution of the absolute magnitudes of CCSNe provides us with information about their progenitors and explosion mechanisms. Richardson et al. (2002) have made a comparative study of the distribution of peak absolute magnitudes in the *B* band (M_B) for various SNe. They have found that for normal and bright Type Ib/c SNe, the mean peak M_B values are -17.61 ± 0.74 and -20.26 ± 0.33 mag, respectively. The M_B values were found to be -17.56 ± 0.38 and -19.27 ± 0.51 mag for normal and bright Type II-L SNe, respectively, while for Type II-P and IIn SNe the M_B values were found to be -17.0 ± 1.12 and -19.15 ± 0.92 mag, respectively.

In a recent study, Li et al. (2011) have derived the absolute magnitudes of Type Ibc (Ib, Ic and Ib/c) and Type II SNe, using Lick Observatory Supernova Search (LOSS) samples. The average absolute magnitudes (close to the *R* band, as claimed by the authors; see the discussion by Li et al. 2011) were found to be -16.09 ± 0.23 and -16.05 ± 0.15 mag for Type Ibc and II SNe, respectively. In a

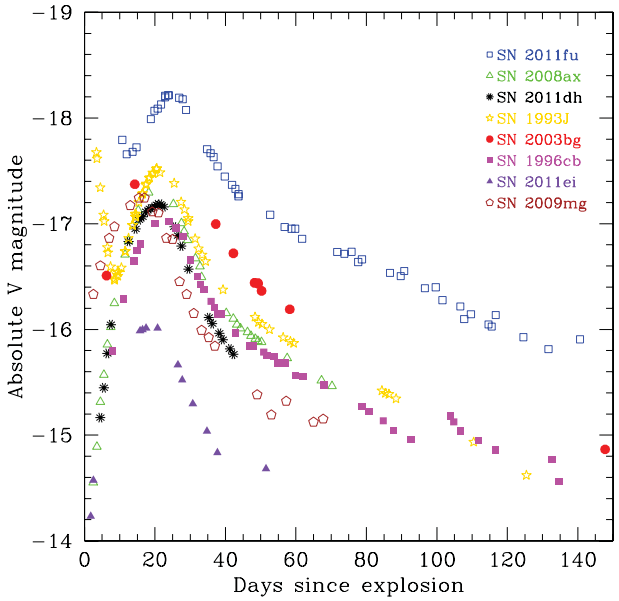

Figure 4. The M_V LC of SN 2011fu is compared with those of other similar Type IIb events: SN 2011ei, 2011dh, 2009mg, 2008ax, 2003bg, 1996cb and 1993J.

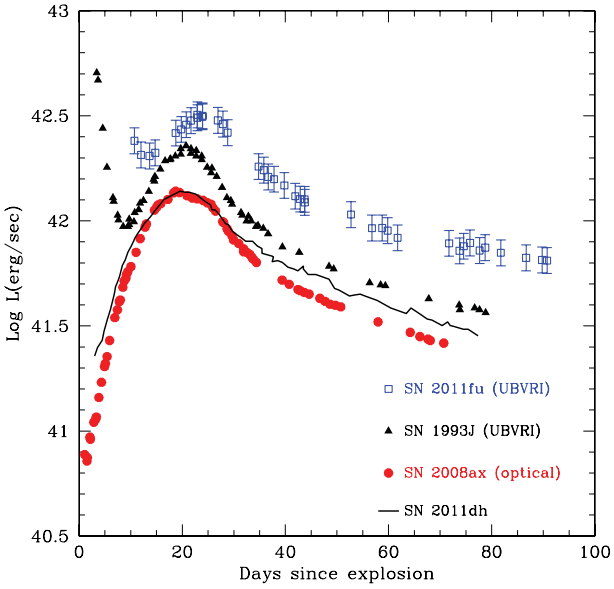

Figure 5. The bolometric LC of SN 2011fu compared with similar Type IIb events: SN 1993J (Lewis et al. 1994), SN 2008ax (Pastorello et al. 2008) and SN 2011dh (Ergon et al., in preparation).

similar study, Drout et al. (2011) have also reported that the *R*-band absolute magnitudes of Type Ib and Ic SNe peak around -17.9 ± 0.9 and -18.3 ± 0.6 mag, respectively.

Fig. 4 shows the comparison of the *V*-band absolute LC of SN 2011fu along with seven other well-observed Type IIb SNe: 1993J (Lewis et al. 1994), 1996cb (Qiu et al. 1999), 2003bg (Hamuy et al. 2009), 2008ax (Pastorello et al. 2008), 2009mg (Oates et al. 2012), 2011dh (Vinkó et al. 2012) and 2011ei (Milisavljevic et al. 2012). For SN 2011fu, the distance $D = 77.9 \pm 5.5$ Mpc has been taken from the NASA/IPAC Extragalactic Data base (NED)[8] along with total $E(B-V) = 0.22 \pm 0.11$ mag, as discussed in Section 3.3. However, all other LCs presented in the figure have been corrected for interstellar extinctions and distance values collected from literature. Fig. 4 illustrates that the peak M_V for various Type IIb SNe has a range between ~ -16 and ~ -18.5 mag. In this distribution, SN 2011fu is the brightest from early to late epochs with a peak absolute magnitude of $M_V \sim -18.5 \pm 0.24$ mag.

4 BOLOMETRIC LIGHT CURVE

4.1 Construction of the bolometric light curve

The quasi-bolometric LC (*UBVRI*) was computed by integrating the extinction-corrected flux[9] in all five bands. The data were interpolated wherever it was necessary and the total *UBVRI* flux was integrated using a simple trapezoidal rule.

In Fig. 5, we compare the quasi-bolometric LC of SN 2011fu along with other three Type IIb events: SNe 1993J (Lewis et al. 1994), 2008ax (Pastorello et al. 2008) and SN 2011dh (Ergon et al., in preparation). It is obvious that the shape of the quasi-bolometric LC of SN 2011fu is similar to that of SN 1993J. However, SN 2011fu is more luminous in comparison with the other SNe during the observed phases.

The unobserved part of the bolometric LC in the infrared (IR) was approximated by assuming blackbody flux distributions fitted to the observed *R*- and *I*-band fluxes for each epoch. First, we used the Rayleigh–Jeans approximation for the fluxes redward of the *I* band, and integrated the flux distribution between the *I*-band central wavelength and infinity. This resulted in an analytical estimate for the IR contribution as $L_{\rm IR} \approx \lambda_I F_I/3$, where λ_I and F_I are the *I*-band central wavelength and monochromatic flux, respectively. Secondly, we fitted a blackbody to the *R*- and *I*-band fluxes at each epoch, and numerically integrated the fitted blackbody flux distributions from the *I* band to radio wavelengths ($\sim$1 mm). These two estimates gave consistent results within a few per cent, which convinced us that they are more or less realistic estimates of the IR contribution. Because the *R*-band fluxes might also be affected by the presence of Hα, we have adopted the result of the first, analytical estimate as the final result. The comparison of the integrated *UBVRI* and IR fluxes has shown that the IR contribution was $\sim$20 per cent at the earliest observed phases, but it increased up to $\sim$50 per cent by day $+40$ and remained roughly constant after that.

4.2 Bolometric light-curve modelling

The bolometric LC (see Section 4.1) was fitted by the semi-analytical LC model of Arnett & Fu (1989) (see also Chatzopoulos, Wheeler & Vinko 2009). This model assumes homologously expanding spherical ejecta having constant opacity, and solves the photon diffusion equation taking into account the laws of thermodynamics. This approach was first introduced by Arnett (1980, 1982), and further extended by Arnett & Fu (1989) by taking into account the rapid change of the opacity due to recombination. The extended diffusion–recombination model was successfully applied to describe the observed LC of SN 1987A, assuming realistic physical parameters (Arnett & Fu 1989).

[8] http://ned.ipac.caltech.edu/

[9] Fluxes were corrected for interstellar reddening using the IDL program *ccm_unred.pro* available at ASTROLIB (http://idlastro.gsfc.nasa.gov/ftp/) by adopting $E(B-V) = 0.22$ mag for the total (Milky Way plus in-host) reddening, and by assuming a reddening law for the diffused interstellar medium ($R_{\rm v} = 3.1$).

The bolometric LC of SN 2011fu is qualitatively similar to that of SN 1987A, because of the presence of the rapid initial decline and the secondary bump, after which the LC settles down on to the radioactive tail as a result of the ^{56}Co decay. This early LC decline in not unusual in Type IIb SNe (however, see Fig. 2 at early epoch where we compare the LCs of SN 2011fu with SN 1993J), and it is usually modelled by a two-component ejecta configuration: a dense compact core and a more extended, lower density envelope on top of the core (Bersten et al. 2012). The fast, initial decline is thought to be a result of the radiation of the cooling outer envelope (which was initially heated by the shock wave passing through it after the explosion), while the secondary bump is caused by the photons diffusing slowly out from the inner, denser ejecta, which is mainly heated from inside by the radioactive decay of ^{56}Ni $\rightarrow$ ^{56}Co $\rightarrow$ ^{56}Fe. After the secondary maximum, the decline of the LC is faster than the rate of the radioactive decay, which might be because of a recombination front moving inward into the ejecta, similar to the condition at the end of the plateau phase in Type II-P SNe.

In order to simulate this type of LC behaviour, we slightly modified the original diffusion–recombination model of Arnett & Fu (1989). Instead of having a H-rich, one-component ejecta, we added an extended, low-density, pure H envelope on top of a denser, He-rich core. Following Arnett & Fu (1989), we have also assumed that the opacity is a result of only Thompson scattering, and it is constant in both the envelope and the core. Because the envelope was thought to contain only H, $\kappa = 0.4$ cm^2 g^{-1} was selected as the Thompson-scattering opacity for this layer, while $\kappa = 0.24$ cm^2 g^{-1} was applied for the inner region to reflect its higher He/H ratio.

The system of differential equations given by Arnett & Fu (1989) were then solved by simple numerical integration (assuming a short, $\Delta t = 1$ s time-step, which was found to be small enough to obtain a reasonable and stable solution). Because the photon diffusion time-scale is much lower in the envelope than in the core, the contribution of the two regions to the overall LC is well separated. During the first few days, the radiation from the outer, adiabatically cooling envelope dominates the LC, while after that only the photons diffusing out from the centrally heated inner core contribute. Thus, the sum of these two processes determines the final shape of the LC.

Because of the relatively large number of free parameters, we have not attempted a formal χ^2 minimization while fitting the model to the observations. Instead, we searched for a qualitative agreement between the computed and observed bolometric LCs. The parameters of our final, best-fitting-by-eye model are collected in Table 6, while the LCs are plotted in Fig. 6.

It is seen that the best-fitting model consists of a dense, 1-M$_\odot$ He-rich core and a more extended, low-mass (0.1 M$_\odot$) H-envelope. This is very similar to the progenitor configuration found by Bersten et al. (2012) when modelling the LC of another Type IIb event, SN 2011dh, although they have assumed a more massive ($\sim$ 3 M$_\odot$) He-core. Nevertheless, Bersten et al. (2012) have concluded – and we have confirmed in the present study – that the secondary bump is entirely a result of radiation coming from the dense inner core of the ejecta, and the outer extended envelope is only responsible for the initial fast decline of the LC. The estimated ejecta mass for SN 2011fu, $\sim$1.1 M$_\odot$, is consistent with the observed rise time ($\sim$24 d) to the secondary maximum of the LC (see equation 10 of Chatzopoulos, Wheeler & Vinko 2012). The parameters in Table 6 are also qualitatively similar to those derived by Young, Baron & Branch (1995) for modelling the LC of SN 1993J.

There are a number of caveats in the simple diffusion–recombination model used above, which naturally limit the accuracy of the derived physical parameters. The most obvious limitation is the assumption of constant opacity in the ejecta. The pre-selected density and temperature profiles in the ejecta (assumed to be exponential functions) are also strong simplifications, but they enable the approximate, semi-analytical treatment of the complex problem of radiative diffusion, as shown by Arnett & Fu (1989). Thus, the parameters in Table 6 can be considered only as order-of-magnitude estimates, which could be significantly improved by more sophisticated modelling codes (e.g. Bersten et al. 2012).

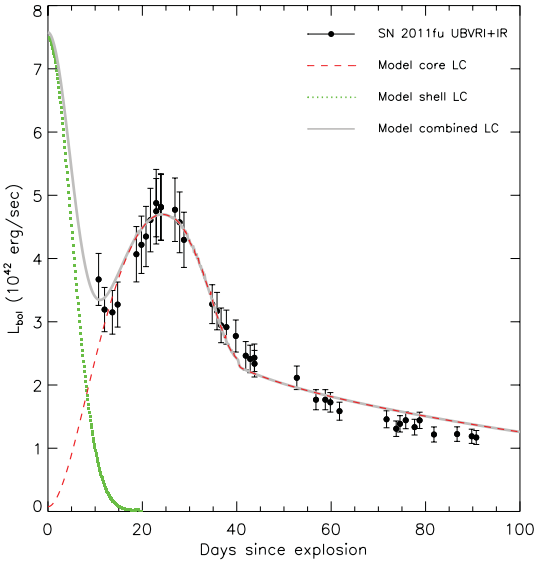

Figure 6. Comparison of the observed bolometric LC (dots) with the best-fitting two-component diffusion-recombination model. The dashed (red) and dotted (green) curves show the contribution from the He-rich core and the low-mass H-envelope, respectively, while the thick (grey) curve gives the combined LC.

Table 6. Log of parameters derived from bolometric light curve modelling, discussed in Section 4.2.

Parameters	He-core	H-envelope	Remarks
R_{prog} (cm)	2×10^{11}	1×10^{13}	Progenitor radius
M_{ej} (M$_\odot$)	1.1	0.1	Ejecta mass
κ_T (cm^2 g^{-1})	0.24	0.4	Thompson scattering opacity
M_{Ni} (M$_\odot$)	0.21	–	Initial nickel mass
E_{kin} (10^{51} erg)	2.4	0.25	Ejecta kinetic energy
$E_{th}(0)$ (10^{51} erg)	1.0	0.3	Ejecta initial thermal energy

5 SPECTRAL ANALYSIS

The properties of the SN 2011fu ejecta have been investigated with the multiparametric resonance scattering code SYNOW (Fisher et al. 1997) (see also Branch et al. 2002; Baron et al. 2005; Elmhamdi et al. 2006). The evolution of temperature and velocities of layers were traced through several months of spectral observations. The SYNOW code is based on several assumptions: spherical symmetry; homologous expansion of layers ($v \sim r$); a sharp photosphere producing a blackbody spectrum and associated with a shock wave at early stages.

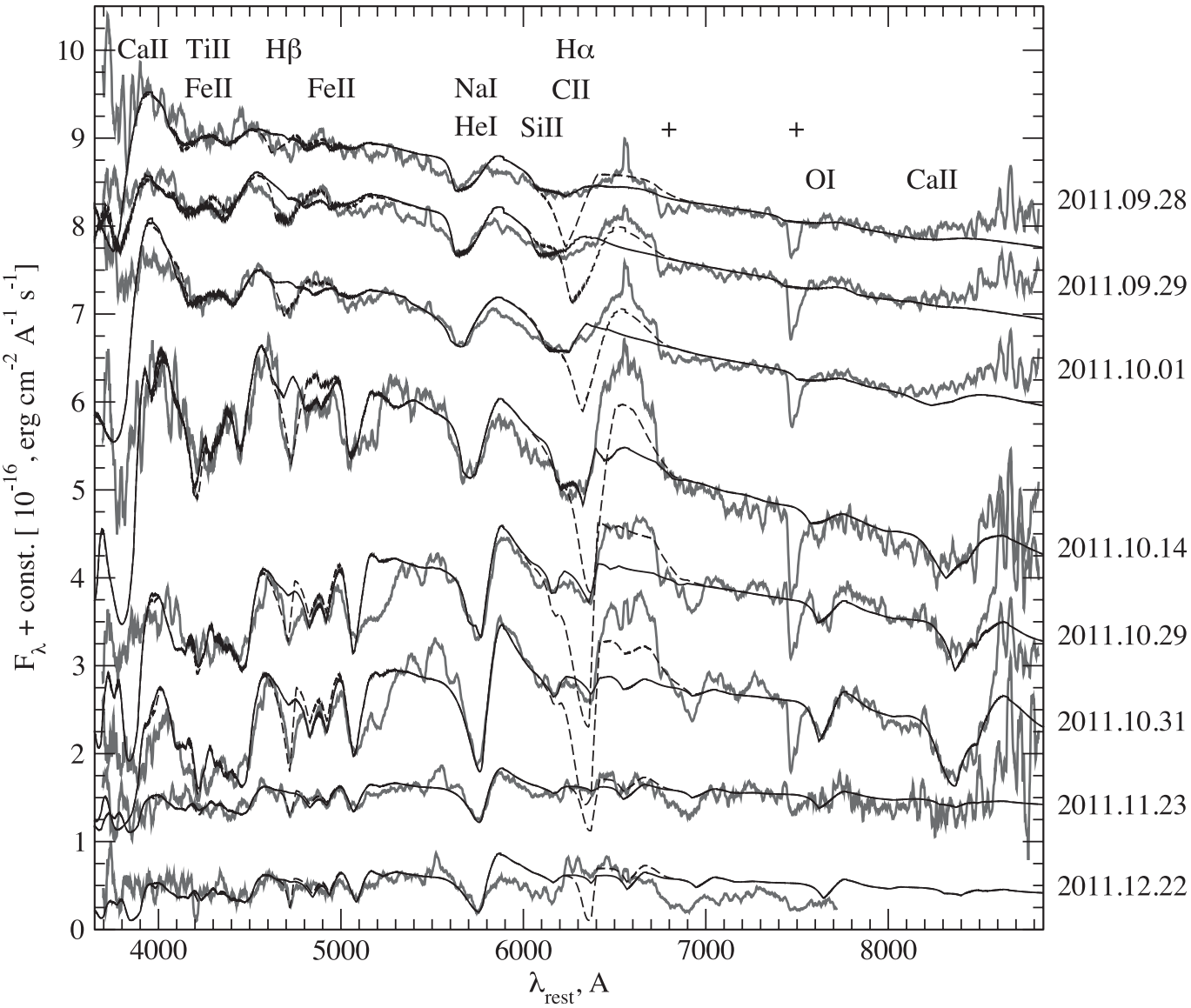

Figure 7. The evolution of the SN 2011fu spectra (grey thick curves, smoothed by a 20-Å-wide window function) overplotted with SYNOW models. The main models are shown by the solid black line. The models with Hβ fitting are shown as a dashed black line. The most conspicuous ions are marked. Atmospheric lines are marked with '+'.

5.1 Comparison between observed and synthetic spectra

In the photospheric phase, the spectral lines with P Cygni profiles are formed by resonance scattering in a shell above the optically thick photosphere, which produces the continuum (see Branch, Baron & Jeffery 2001). However, during the nebular phase, the ejecta are transparent (optically thin) in the optical wavelength range. In this case, the spectrum is dominated by strong emission features, including forbidden lines. Each of these two phases of SN evolution can be explained with individual approximations, and the modelling of the observed spectra should be made with different synthetic codes. There is no sharp boundary between these two phases. No strong transition to the nebular phase with conspicuous emission features can be seen in the observed spectra of SN 2011fu (Fig. 7). The shape of lines remains the P Cyg profile, which suggests that they are formed by resonance scattering, as assumed in SYNOW. Thus, we have modelled all the spectra of SN 2011fu with this code. Before modelling, all spectra have been corrected for redshift (see Section 2).

The strong emission component of the Hα line (probably with C II and Si II contamination) cannot be fully fitted in the terms of the SYNOW code. We have focused primarily on the absorption parts of P Cyg line profiles, which provide information about the expansion velocities of different line-forming layers. The SYNOW code allows us to use different optical depth (i.e. density) profiles. Two of these are the exponential profile with the parameter of e-folding velocity v_e, $\tau \propto \exp(-v/v_e)$, which can be adjusted for each ion, and the power-law profile with the index n, $\tau \propto v^{-n}$, which is applied to all ions in the model. We have checked both cases and have found that the exponential law is more suitable for our spectra. Both the original paper of the SYNOW developers and further studies have shown the possibility of spectral features, which can be detached or undetached

Table 7. Velocities of the pseudo-photosphere, Hα and Hβ for different epochs of SN 2011fu evolution, derived with SYNOW. We have assumed that the photospheric velocity (V_{phot}) is equal to the velocity of Fe II. All velocities are given in km s^{-1}. T_{bb} is the blackbody temperature of the pseudo-photosphere in Kelvin. The colour temperature (T_{col}) derived from the effective temperature–colour relations (see Dessart & Hillier 2005; Bersten & Hamuy 2009) is given in the last column.

UT date (yyyy/mm/dd)	V_{phot} (Fe II)	V(Hα)	V(Hβ)	T_{bb}	T_{col}
2011/09/28	14 000	16 000	16 000	6700	6952
2011/09/29	14 000	16 000	14 000	6500	6476
2011/10/01	11 000	15 000	11 000	6500	6052
2011/10/14	8000	11 000	8500	6700	5791
2011/10/29	6200	9500	9500	5000	4698
2011/10/31	6000	9000	9000	5000	4795
2011/11/23	6000	9000	9000	5000	5094
2011/12/22	5000	9000	9000	5000	5718

from the photosphere. These two configurations produce different shapes for the line profiles, as described by Sonbas et al. (2008).

The first three observed spectra are separated by only 1 and 2 d. This is the reason why they can be modelled by similar sets of parameters (see Table 7). Even the spectrum obtained on October 14 has a similar continuum slope ($T_{bb} \approx$ 6500–6700 K). To verify the pseudo-photospheric temperature derived by SYNOW modelling, we have also evaluated the colour temperature (T_{col}) of the SN using the models of Dessart & Hillier (2005) and Bersten & Hamuy (2009). We have used the $B - V$ colours for those epochs where spectra are available, and then we have estimated the temperature from the corresponding $B - V$ colour. Both of these temperature estimates seem to be consistent, except for the spectra taken on 2011 October 14 and December 22.

5.2 Velocity of the pseudo-photosphere

The velocity of the pseudo-photosphere (an optically thick layer, the surface of last scattering for continuum photons) can be located by velocities of heavy elements, such as Fe II and Ti II, which might produce optically thin spectral features. However, during the very early phases, these features are very weak and blended. Therefore, fitting the first three spectra by these ions gives a wide range of possible photospheric velocities, extending from 13 000 to 19 000 km s^{-1}. The most prominent, narrow absorption feature in these spectra is the feature near 5650 Å produced by He I (which might be blended with Na I D). This feature is useful to better constrain the velocity at the pseudo-photosphere, and to decrease the uncertainty of this parameter at the earliest phases. All velocities derived in this way are shown in the V_{phot} column of Table 7.

5.3 Hydrogen and the 6200-Å absorption feature

The wide absorption feature near 6200 Å can be fitted with the help of a high-velocity H-layer (up to $V \sim 20\,000$ km s^{-1}), which might be detached from the pseudo-photosphere. However, in order to fit the emission peak of Hα with SYNOW, we need lower velocities, but those models cannot reproduce the absorption profile (see Fig. 7). In the V(Hα) column of Table 7, we list the results from the latter, more conservative solution.

The broad absorption at 6200 Å can also be explained by the presence of the C II ion having a high velocity almost identical to that of Hα. Moreover, C II also produces a small feature near 4400 Å. This feature can constrain the reference optical depth (τ) for ionized carbon. However, the contamination from heavy elements in the blue region makes the fitting of the C II 4400-Å feature uncertain. Thus, the presence of carbon cannot be confirmed from these spectra.

It is also possible to explain the 6200-Å feature by singly ionized silicon. In this case, the velocity of Si II must be very low. However, it is expected that the velocity of Si II should be equal or only slightly higher than the photospheric velocity. We have found that only the blue wing of this wide feature can be fitted by Si II. Although the small absorption near 5880 Å might be explained by the presence of Si II, the observed shape of the 6200 Å feature does not confirm this hypothesis.

In order to look for other possibilities, we have also checked different blends of H, Si II, C II and some other ions with different velocities (assuming undetached as well as detached line formation) in our models. At the early phases, we found the range of derived velocities to be wide because of the lack of observable spectral features formed close to the photosphere, as discussed above. At the late phases, the wide absorption near 6200 Å split into at least three separate features: 6100, 6200 and 6350 Å. These features might be explained as a line-formation effect for Hα in layers with different velocities or the appearance of blending because of ions, as mentioned above. Unfortunately, no firm conclusion can be drawn based on the simple parametric models that SYNOW can produce.

The deep absorption near 4700 Å can be naturally explained by identifying it as the Hβ line. We fitted this line and the Hα line independently because they cannot be modelled by the same set of parameters: τ, v_{phot} and v_e (see also Quimby et al. 2007). From Table 7, we can see that for the spectra obtained before October 29 the fitting of Hα needs higher velocities than the fitting of Hβ. Although both the Hα and Hβ velocities declined in time, the formation of the absorption component of Hα remained at higher velocities than for Hβ. This might suggest that Hα remained optically thick for a longer time than Hβ in the expanding, diluting H-rich envelope.

5.4 Other ions

To fit the main features in the spectra, we included the following elements and ions in SYNOW: H, Fe II, Ti II, Na I, Si II, O I and Ca II. Some models were also computed containing the following elements and ions as alternatives: C II, He I, Fe I, Ti I, Sc II, Mg I. The consistency of these ions were cross-examined with Hatano et al. (1999). The heavier atoms/ions should have velocities close to v_{phot} but the lighter ones might be detached because of, for example, stratification of elements in the ejecta.

In the following, we show some possible explanations for these features in the observed spectra. Weak features near 4810 and 6370 Å can be explained by the presence of low-velocity He I. He can also be found as a blend with Na I in the deep absorption near 5650 Å, as mentioned above, and as a blend with Ti II and Fe II near 4300 Å. However, the velocity of He I might be higher than the photospheric velocity. Even in this case, the presence of He can explain all these features.

A small absorption in the blue wing of Hα at 6630 Å could be modelled by He I or low-velocity C II. The feature near 5050 Å could also be fitted with Mg I. The Ca II H+K feature cannot be fitted well around 3730 Å, because this regime is at the blue end of our observed spectra and all of the spectra are very noisy at these wavelengths. However, the absorption feature near 8400 Å is compatible with the Ca II IR triplet.

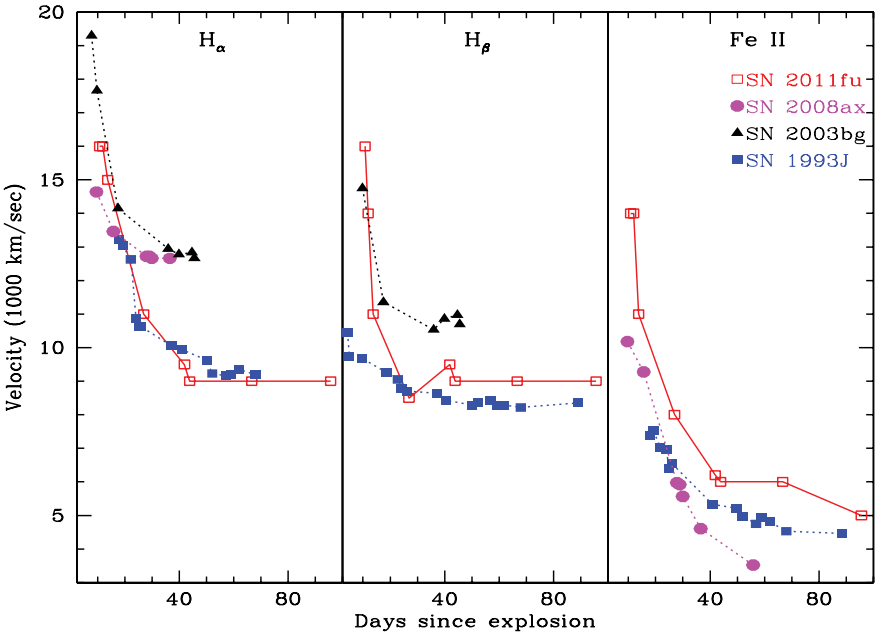

Figure 8. The evolution of Hα, Hβ and Fe II line velocities by fitting the SYNOW model (see Table 7). Photospheric velocities for SN 2011fu, 2003bg (Hamuy et al. 2009), 1993J (Lewis et al. 1994; Barbon et al. 1995) and 2008ax (Pastorello et al. 2008) are shown. The symbols of SN 2011fu are connected with solid lines, and those of other SNe with dotted lines.

5.5 Results of spectral modelling

Almost all the spectral features are described well with elements and ions, which are usually applied for Type IIb SNe. However, the strong emission of Hα, which dominates during intermediate epochs, cannot be fully fitted with the models applied.

The fitting of redder and, especially, bluer parts has some uncertainties because of the strong blending of metal lines such as Ca II, Ti II, Fe II and others. Even without precise modelling, all spectral sequences can be divided into two groups: the first four spectra (up to October 14), which are fitted with models with the blackbody temperature $T_{\rm bb} \approx$ 6500–6700 K, and the following four spectra with $T_{\rm bb} \approx 5000$ K.

Generally, the modelling of the SN 2011fu spectra shows the decline of the photospheric velocities up to ∼40 d after the explosion (see Fig. 8). Then, all velocities remain approximately at the same, stable level. This behaviour was also described in previous works on CCSNe (Branch et al. 2002; Quimby et al. 2007; Moskvitin et al. 2010). In Fig. 8, we plot the velocities of Hα, Hβ and Fe II for SN 2011fu, SN 2008ax, SN 2003bg and SN 1993J, illustrating this effect.

6 METALLICITY–BRIGHTNESS COMPARISON OF HOST GALAXIES

In several earlier studies of CCSNe hosts, it has been already mentioned that various SNe subtypes occur in different environments (see Prieto, Stanek & Beacom 2008; Anderson et al. 2010; Arcavi et al. 2010; Modjaz et al. 2011; Kelly & Kirshner 2012; Sanders et al. 2012). Metallicity is a key factor in all these studies. Recently, Arcavi et al. (2010) and Prieto et al. (2008) have found that Type Ib/c SNe host galaxies are metal-rich, compared to Type II SNe hosts. Modjaz et al. (2011) have found that Type Ic SNe are more metal-rich (up to 0.20 dex) than Type Ib SNe. In a similar study on Type Ib/c SNe locations, Leloudas et al. (2011) have found a smaller gap between the two metallicities (the environment of Type Ic SNe is richer by ∼0.08 dex than Type Ib SNe). In a recent study with a different approach (using the local emission line for metallicity estimates), where 74 H II regions in CCSNe hosts were analysed, Anderson et al. (2010) did not find any difference between the metallicities of these two environments.

Type IIb host galaxies have been claimed to be more metal-poor than those of Type Ib or Ic SNe (see Arcavi et al. 2010; Kelly & Kirshner 2012). However, in another recent study based on the SN sample from untargeted searches (although with a small sample of eight Type IIb SNe), Sanders et al. (2012) have found that the median metallicity of both Type Ib and IIb SNe host galaxies is very similar.

In an attempt to understand the metallicity scenario for the SN 2011fu host galaxy, we have collected the latest sample of metallicity data for hosts of CCSNe, and their absolute magnitudes in the *B* band from the literature (Leloudas et al. 2011; Modjaz et al. 2011; Stoll et al. 2012) and online.[10] In Fig. 9, the data for these host galaxies (36 for Type Ib, 15 for Type IIb and 167 for the remaining Type II SNe) were then overplotted onto the sample containing all star-forming galaxies from the Sloan Digital Sky Survey (SDSS) Data Release 4 (DR4; this sample was taken from Prieto et al. 2008). The relations between metallicity and $M_{\rm B}$ for galaxies from several papers are also overplotted (Skillman, Kennicutt & Hodge 1989; Richer & McCall 1995; Kobulnicky & Zaritsky 1999; Contini et al. 2002; Melbourne & Salzer 2002; Tremonti et al. 2004).

We have estimated the metallicity of the host of SN 2011fu using the relation given by Garnett (2002, see equation 6 of that paper). We have considered $M_{\rm B} = -20.62$ mag for UGC 01626 from HyperLeda. The calculated log (O/H)+12 for UGC 01626 is $8.90^{+0.10}_{-0.06}$. This value is slightly higher than log (O/H)+12 = 8.55 (Arcavi et al. 2010) and log (O/H)+12 = 8.44 (Sanders et al. 2012) for the Type II SNe sample. Our analysis, which uses the most up-to-date sample of absolute magnitudes and metallicities of CCSNe

[10] http://www.astro.princeton.edu/∼jprieto/snhosts/

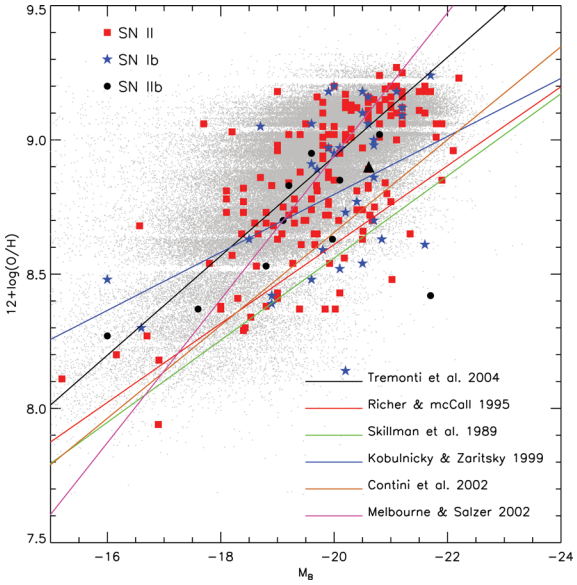

Figure 9. Metallicity–luminosity relation for various types of SNe host galaxies. The tiny dots denote all galaxies used by Prieto et al. (2008) (this catalog is based on the SDSS DR4 data base; Adelman-McCarthy et al. 2006). Red squares are Type II, stars are Type Ib/c and black dots are Type IIb SNe, respectively. The analytical relations collected from several papers (see text) are also overplotted. The host metallicity of SN 2011fu is denoted by a black triangle.

host galaxies, also supports the results described by Sanders et al. (2012). However, it is noticeable that the methods used to determine metallicities are based on statistical samples and are affected by the incompleteness of the sample, and thus should be used with caution.

7 CONCLUSIONS

We have presented a comprehensive *UBVRI* photometric and low-resolution spectroscopic monitoring of the Type IIb SN 2011fu. To date, only a handful of SNe belonging to this class have been observed and studied in detail.

To the best of our knowledge, our photometric and spectroscopic observations described here are the earliest reported for this event. The early photometric observations strongly suggest the presence of the early-time decline of the LC (which is thought to be related to the shock break-out phase) as seen for SN 1993J. The early-time LC decay rate (α_1) of this SN is slower than that derived for SN 1993J in all bands. The rising rates between the LC valley-to-peak (α_2) observed in SN 2011fu is also slower than in SN 1993J. However, the post-peak LC decay rates (α_3) are similar in the two events.

The colour evolutions of SN 2011fu have been studied using our *UBVRI*-band observations. Our data have shown that during the very early phases the $B - V$ colour was very similar to that in SN 1993J. A similar trend has also been found in the $V - R$ and $V - I$ colours. The evolution of these three colours after +40 d was also similar to that seen in other CCSNe. The *V*-band absolute magnitudes of a sample of eight Type IIb SNe were compared after applying proper extinction corrections and taking into account distances collected from the literature. In this sample, SN 2011fu seems to be the most luminous event. However, the peak *V*-band absolute magnitude of SN 2011fu is not an outlier when compared to the peak brightness of CCSNe of other types.

The quasi-bolometric LC of SN 2011fu was assembled using our *UBVRI* data and taking into account the IR contribution, as specified in Section 4. The comparison of these data with other known Type IIb SNe also shows that SN 2011fu is the brightest Type IIb SN in the sample. The bolometric LC was modelled by applying a semi-analytical model of Arnett & Fu (1989). This model suggests a 1.1-$M_\odot$ He-rich core and an extended, low-mass ($\sim$0.1 $M_\odot$) H-envelope as the progenitor of SN 2011fu, similar to that of SN 2011dh. However, the progenitor radius of SN 2011fu ($\sim 1 \times 10^{13}$ cm) has been found to be smaller than that of SN 1993J ($\sim 4 \times 10^{13}$ cm; Woosley et al. 1994). The ejected nickel mass for SN 2011fu was $\sim$0.21 $M_\odot$, higher than that of SN 1993J (0.07–0.11 $M_\odot$).

The spectra of SN 2011fu taken at eight epochs have been analysed using the multiparameter resonance scattering code SYNOW. The derived parameters describe the evolution of the velocities related to various atoms/ions and the variation of the blackbody temperature of the pseudo-photosphere. The photospheric velocities at the early epochs were higher than that of other Type IIb SNe. The pseudo-photospheric temperatures were found to be between 6700 and 5000 K, decreasing from initial to later phases. The temperatures from SYNOW were also checked by comparing them with colour temperatures calculated from $B - V$ versus $T_{\rm eff}$ relations (Dessart & Hillier 2005; Bersten & Hamuy 2009). These different temperature estimates were found to be consistent. The appearances of the main observed spectral features were also successfully modelled with SYNOW by assuming H, He I and various metals (mostly Fe II, Ti II and Ca II), which are typical of CCSNe spectra. The estimated value of the metallicity of the host galaxy of SN 2011fu is $8.90^{+0.10}_{-0.06}$, similar to those for other Type IIb SNe.

ACKNOWLEDGEMENTS

We thank the referee, Andrea Pastorello, for a critical reading of the paper and for several useful comments and suggestions that have greatly improved the scientific content of the manuscript. We are also grateful to the observers at the Aryabhatta Research Institute of Observational Sciences (ARIES), who provided their valuable time and support for the observations of this event. We are grateful to the staff of the 1.3-m DFOT and HCT for their kind cooperation. SBP acknowledges the support of the Indo-Russian (DST-RFBR) project No. INT/RFBR/P-100 for this work. This work was also supported by the following grants: RFBR grant 11-02-12696-IND-a; program no. 17 'Active processes in galactic and extragalactic objects' of the Department of Physical Sciences of the Russian Academy of Sciences; grants No. 14.B37.21.0251 and No. 14.A18.21.1179 from the Federal Targeted Programme of the Ministry of Education and Science of the Russian Federation. The work of JV and AO has been supported by Hungarian OTKA Grant K76816. BK is grateful to C. Eswaraiah, for his help during the writing of this paper. BK also acknowledges the support of Actions de Recherche Concertées (ARC). This research has made use of the NED, which is operated by the Jet Propulsion Laboratory, California Institute of Technology, under contract with the National Aeronautics and Space Administration. We acknowledge the use of the HyperLeda data base (http://leda.univ-lyon1.fr).

REFERENCES

Adelman-McCarthy J. K. et al., 2006, ApJS, 162, 38
Aldering G., Humphreys R. M., Richmond M., 1994, AJ, 107, 662
Anderson J. P., James P. A., 2009, MNRAS, 399, 559
Anderson J. P., Covarrubias R. A., James P. A., Hamuy M., Habergham S. M., 2010, MNRAS, 407, 2660

Arcavi I. et al., 2010, ApJ, 721, 777
Arcavi I. et al., 2011, ApJ, 742, L18
Arnett W. D., 1980, ApJ, 237, 541
Arnett W. D., 1982, ApJ, 253, 785
Arnett W. D., Fu A., 1989, ApJ, 340, 396
Barbon R., Benetti S., Cappellaro E., Patat F., Turatto M., Iijima T., 1995, A&AS, 110, 513
Baron E., Nugent P. E., Branch D., Hauschildt P. H., 2005, in Turatto M., Benetti S., Zampieri L., Shea W., eds, ASP Conf. Ser. Vol. 342, 1604–2004: Supernovae as Cosmological Lighthouses. Astron. Soc. Pac., San Francisco, p. 351
Benetti S., Cappellaro E., Turatto M., Pastorello A., 2000, IAU Circ., 7375, 2
Bersten M. C., Hamuy M., 2009, ApJ, 701, 200
Bersten M. C. et al., 2012, ApJ, 757, 31
Bietenholz M. F., Brunthaler A., Soderberg A. M., Krauss M., Zauderer B., Bartel N., Chomiuk L., Rupen M. P., 2012, ApJ, 751, 125
Blinnikov S. I., Eastman R., Bartunov O. S., Popolitov V. A., Woosley S. E., 1998, ApJ, 496, 454
Blondin S., Tonry J. L., 2007, ApJ, 666, 1024
Branch D., Baron E., Jeffery D. J., 2001, in Weiler K. W., ed., Lecture Notes in Physics, Vol. 598, Supernovae and Gamma-Ray Bursters. Springer, New York, p. 47 (astro-ph/0111573)
Branch D. et al., 2002, ApJ, 566, 1005
Chatzopoulos E., Wheeler J. C., Vinko J., 2009, ApJ, 704, 1251
Chatzopoulos E., Wheeler J. C., Vinko J., 2012, ApJ, 746, 121
Chevalier R. A., 1992, ApJ, 394, 599
Chevalier R. A., Fransson C., 2008, ApJ, 683, L135
Chevalier R. A., Soderberg A. M., 2010, ApJ, 711, L40
Chornock R. et al., 2011, ApJ, 739, 41
Ciabattari F. et al., 2011, Central Bureau Electronic Telegrams, 2827, 1
Clocchiatti A. et al., 1997, ApJ, 483, 675
Contini T., Treyer M. A., Sullivan M., Ellis R. S., 2002, MNRAS, 330, 75
Crockett R. M. et al., 2008, MNRAS, 391, L5
Dessart L., Hillier D. J., 2005, A&A, 437, 667
Drout M. R. et al., 2011, ApJ, 741, 97
Elmhamdi A., Danziger I. J., Branch D., Leibundgut B., Baron E., Kirshner R. P., 2006, A&A, 450, 305
Falk S. W., Arnett W. D., 1977, ApJS, 33, 515
Filippenko A. V., 1988, AJ, 96, 1941
Filippenko A. V., 1997, ARA&A, 35, 309
Filippenko A. V., Chornock R., 2003, IAU Circ., 8084, 4
Fisher A., Branch D., Nugent P., Baron E., 1997, ApJ, 481, L89
Fryer C. L., 1999, ApJ, 522, 413
Gal-Yam A. et al., 2011, ApJ, 736, 159
Garnett D. R., 2002, ApJ, 581, 1019
Hamuy M. et al., 2009, ApJ, 703, 1612
Hatano K., Branch D., Fisher A., Millard J., Baron E., 1999, ApJS, 121, 233
Heger A., Fryer C. L., Woosley S. E., Langer N., Hartmann D. H., 2003, ApJ, 591, 288
Horesh A. et al., 2012, preprint (arXiv:1209.1102)
Horne K., 1986, PASP, 98, 609
Kelly P. L., Kirshner R. P., 2012, ApJ, 759, 107
Kobulnicky H. A., Zaritsky D., 1999, ApJ, 511, 118
Krauss M. I. et al., 2012, ApJ, 750, L40
Kumar B., Sagar R., Rautela B. S., Srivastava J. B., Srivastava R. K., 2000, Bull. Astron. Soc. India, 28, 675
Landolt A. U., 2009, AJ, 137, 4186
Leloudas G. et al., 2011, A&A, 530, A95
Lewis J. R. et al., 1994, MNRAS, 266, L27
Li W. et al., 2011, MNRAS, 412, 1441
Martí-Vidal I. et al., 2011, A&A, 535, L10
Maund J. R., Smartt S. J., Kudritzki R. P., Podsiadlowski P., Gilmore G. F., 2004, Nat, 427, 129
Maund J. R. et al., 2011, ApJ, 739, L37
Maurer I., Mazzali P. A., Taubenberger S., Hachinger S., 2010, MNRAS, 409, 1441
Mazzali P. A., Deng J., Hamuy M., Nomoto K., 2009, ApJ, 703, 1624
Melbourne J., Salzer J. J., 2002, AJ, 123, 2302
Milisavljevic D. et al., 2012, preprint (arXiv:1207.2152)
Modjaz M., Kewley L., Bloom J. S., Filippenko A. V., Perley D., Silverman J. M., 2011, ApJ, 731, L4
Monard L. A. G., 2007, Central Bureau Electronic Telegrams, 845, 1
Moskvitin A. S., Sonbas E., Sokolov V. V., Fatkhullin T. A., Castro-Tirado A. J., 2010, Astrophys. Bull., 65, 132
Munari U., Zwitter T., 1997, A&A, 318, 269
Nakar E., Sari R., 2010, ApJ, 725, 904
Oates S. R. et al., 2012, MNRAS, 424, 1297
Pastorello A. et al., 2008, MNRAS, 389, 955
Podsiadlowski P., Joss P. C., Hsu J. J. L., 1992, ApJ, 391, 246
Prieto J., 2009, Central Bureau Electronic Telegrams, 2087, 1
Prieto J. L., Stanek K. Z., Beacom J. F., 2008, ApJ, 673, 999
Puls J., Vink J. S., Najarro F., 2008, A&A Rev., 16, 209
Qiu Y., Li W., Qiao Q., Hu J., 1999, AJ, 117, 736
Quimby R. M., Wheeler J. C., Höflich P., Akerlof C. W., Brown P. J., Rykoff E. S., 2007, ApJ, 666, 1093
Richardson D., Branch D., Casebeer D., Millard J., Thomas R. C., Baron E., 2002, AJ, 123, 745
Richardson D., Branch D., Baron E., 2006, AJ, 131, 2233
Richer M. G., McCall M. L., 1995, ApJ, 445, 642
Richmond M. W., Treffers R. R., Filippenko A. V., Paik Y., Leibundgut B., Schulman E., Cox C. V., 1994, AJ, 107, 1022
Roming P., Prieto J., Milne P. A., 2009a, Central Bureau Electronic Telegrams, 2093, 1
Roming P. W. A. et al., 2009b, ApJ, 704, L118
Roming P. et al., 2010, Bull. Am. Astron. Soc., 42, 448
Ryder S. D., Murrowood C. E., Stathakis R. A., 2006, MNRAS, 369, L32
Sagar R. et al., 2011, Current Science, 101 (08)
Sagar R., Kumar B., Omar A., Joshi C., 2012, in Astron. Soc. India Conf. Ser. Vol. 4, p. 173
Sanders N. E. et al., 2012, ApJ, 758, 132
Schlegel D. J., Finkbeiner D. P., Davis M., 1998, ApJ, 500, 525
Schmidt B. P. et al., 1993, Nat, 364, 600
Shigeyama T., Suzuki T., Kumagai S., Nomoto K., Saio H., Yamaoka H., 1994, ApJ, 420, 341
Skillman E. D., Kennicutt R. C., Hodge P. W., 1989, ApJ, 347, 875
Smartt S. J., 2009, ARA&A, 47, 63
Soderberg A. M., Chevalier R. A., Kulkarni S. R., Frail D. A., 2006, ApJ, 651, 1005
Soderberg A. M. et al., 2012, ApJ, 752, 78
Sonbas E. et al., 2008, Astrophys. Bull., 63, 228
Stetson P. B., 1987, PASP, 99, 191
Stetson P. B., 1992, in Worrall D. M., Biemesderfer C., Barnes J., eds, ASP Conf. Ser. Vol. 25, Astronomical Data Analysis Software and Systems I. Astron. Soc. Pac., San Francisco, p. 297
Stoll R., Prieto J. L., Stanek K. Z., Pogge R. W., 2012, preprint (arXiv:1205.2338)
Stritzinger M., 2010, Central Bureau Electronic Telegrams, 2158, 1
Stritzinger M. et al., 2009, ApJ, 696, 713
Taubenberger S. et al., 2011, MNRAS, 413, 2140
Tomasella L., Valenti S., Ochner P., Benetti S., Cappellaro E., Pastorello A., 2011, Central Bureau Electronic Telegrams, 2827, 2
Tremonti C. A. et al., 2004, ApJ, 613, 898
Van Dyk S. D. et al., 2011, ApJ, 741, L28
Vinkó J. et al., 2012, A&A, 540, A93
Waxman E., Mészáros P., Campana S., 2007, ApJ, 667, 351
Wheeler J. C. et al., 1993, ApJ, 417, L71
Woosley S., Janka T., 2005, Nature Physics, 1, 147
Woosley S. E., Pinto P. A., Martin P. G., Weaver T. A., 1987, ApJ, 318, 664
Woosley S. E., Eastman R. G., Weaver T. A., Pinto P. A., 1994, ApJ, 429, 300
Young T. R., Baron E., Branch D., 1995, ApJ, 449, L51

This paper has been typeset from a TEX/LATEX file prepared by the author.